SMALL DISTURBANCE NAVIER-STOKES METHOD: AN EFFICIENT TOOL FOR PREDICTING UNSTEADY AIR LOADS

Alexander Pechloff * **, Boris Laschka** †
Institute for Fluid Mechanics, Aerodynamics Division, Technische Universität München,
Boltzmannstr. 15, D-85747 Garching, Germany

Keywords: *small disturbance Navier-Stokes equations, computational fluid dynamics, aeroelasticity*

Abstract

In regard to aeroelastic applications the otherwise common yet computationally expensive approach of time-accurately solving the unsteady Reynolds-averaged Navier-Stokes equations is not feasible. However, a numerical method based on the small disturbance formulation of these governing equations, as presented here, can provide an efficient and accurate tool for predicting aerodynamic loading. The triple decomposition, which separates unsteady flow into a steady mean part, a periodic perturbation and a turbulent component, serves as the theoretical basis for their derivation. Assuming the periodic perturbation is small in comparison to the mean flow, higher order perturbation terms emerging through the decomposition process of the instantaneous Navier-Stokes equations are disregarded. Furthermore, arising turbulent correlation terms are approximated through an eddy viscosity approach, yielding the time-linearized governing equations for perturbed flow at high Reynolds number. The Spalart-Allmaras turbulence model is selected for describing the perturbed as well as the mean eddy viscosity throughout the flow field. With the restriction of the time dependent quantities to harmonic behavior the linearized perturbed flow equations are recast in the frequency domain as the small disturbance Navier-Stokes equations. Thus, the initial unsteady problem is reduced to a steady one for the perturbation part. Insight into the numerical aspects of the small disturbance Navier-Stokes method (FLM-SD.NS) is provided in a compact manner. Initial validation of FLM-SD.NS is performed with a harmonically pitching NACA 64A010 airfoil in transonic turbulent flow. Computational results are in good agreement with experimental data, as well as time-accurate Reynolds-averaged Navier-Stokes solutions provided by the comparative solver FLM-NS and FLOWer. Reductions in computational time up to an order of magnitude in comparison to FLM-NS are observed.

1 Introduction

Within the aeroelastic analysis process a thorough investigation of the effects of unsteady air loads on lifting structures demands the broad variation of such parameters as Mach number, Reynolds number, incidence angle, amplitude, frequency and eigenmode. When employing conventional time-accurate Euler or Reynolds-averaged Navier-Stokes methods, computational effort for the necessary permutations becomes prohibitively high. As periodicity of the flow is obtained only after having calculated a number of cycles per case, simulations at low frequencies become especially time consuming. Historically, the inherent problem of computational cost has been dealt with by utilizing methods relying

* Dipl.-Ing. Univ., Research Assistant

† Prof. em. Dr.-Ing.

on less complex flow models. Inviscid numerical solutions of the linear potential, transonic small disturbance or full potential equations are efficiently calculated and nowadays in widespread aeroelastic use. In recent years such approaches have been supplemented by the introduction of small disturbance Euler methods, which provide inviscid flow modelling of a higher order, while retaining an efficient solution process.

Originating from the field of turbomachinery, principal investigations based on the small disturbance Euler equations were perfomed by Hall and Crawley [9] for flutter/forced response in two-dimensional cascade flows. Under the assumption of harmonic motion a frequency fomulation yields linear variable coefficient equations for the complex amplitude of the field quantities. Consequently, the elimination of the time dependency allows for an efficient numerical integration and supports the customary aeroelastic modal methods. Furthermore, Lindquist and Giles [15] have shown the suitability of the small disturbance Euler equations for providing high quality resolution of transonic discontinuities.

A succesful transfer of this approach to the external flow problem in the field of aircraft aerodynamics was realized at the Institute for Fluid Mechanics (Technische Universität München), where the small disturbance Euler solver FLM-SDEu was developed by Kreiselmaier [12]. Validation results for select airfoils and wings performing pitching motions in the sub-, trans- and supersonic flow regime have demonstrated the ability of FLM-SDEu to provide a fast means for accurately predicting unsteady forces. In the continuing process of establishing FLM-SDEu as a common aeroelastic tool, cooperation with the aircraft industry has resulted in various studies regarding the unsteady air loads associated with a high performance aircraft wing. Specifically, the aerodynamic effects of various eigenmodes [22], of rigid body motions [25], as well as flap efficiency with [25] and without external store [2] have been investigated using FLM-SDEu.

Unfortunately, the afore mentioned inviscid methods reach their limitation when confronted with flow fields exhibiting significant viscous effects, such as flow separation or shock boundary layer interaction. As even efficient approaches based on viscous-inviscid coupling possess evident shortcomings in such cases and traditional time domain solutions of the Reynolds-averaged Navier-Stokes equations become unwieldly, extension of a small disturbance Euler method to viscous flow becomes a promising alternative. Once again, the development of a numerical solver based on the the small-disturbance Navier-Stokes equations was pioneered by the turbomachinery sector, where Clark and Hall [6] initially utilize such a method for investigating stall flutter in two-dimensional cascades and prove its feasibility. Recently, the German Aerospace Center (DLR) has taken up and extended this approach [21]. As the application to the field of aircraft aerodynamics becomes reasonable, the small disturbance Navier-Stokes method FLM-SD.NS is developed from the existing inviscid solver FLM-SDEu by supplementing the additional viscous algorithms. Additionally, the treatment of high Reynolds number flow requires the incorporation of a turbulence model in appropriate formulation. The initial study is restricted to two-dimensional flows.

2 Theory

2.1 The Navier-Stokes Equations

Unsteady compressible viscous flow is governed by the Navier-Stokes equations. Accounting for mesh movement, the system of partial differential equations are expressed in non-dimensionalized strong conservation form for a body fitted curvilinear coordinate system:

$$\frac{\partial \mathbf{Q}}{\partial \tau} + \frac{\partial \mathbf{F}}{\partial \xi} + \frac{\partial \mathbf{G}}{\partial \eta} = \frac{\partial \mathbf{F}_v}{\partial \xi} + \frac{\partial \mathbf{G}_v}{\partial \eta}. \tag{1}$$

Denoting the determinant of the coordinate transformation's Jacobian with $J = x_\xi y_\eta - x_\eta y_\xi$, the curvilniear state vector of conservative variables $\mathbf{Q}$ is specified in relationship to its Cartesian counterpart $\mathbf{q}$ as

$$\mathbf{Q} = J\mathbf{q} = J\left(\rho, \rho u, \rho v, \rho e\right)^T. \tag{2}$$

Density ρ, the velocity components u and v in Cartesian x- and y-direction, as well as the specific total energy e are identified as the primitive dependent variables composing $\mathbf{q}$. Non-dimensional time is represented by τ. The vectors $\mathbf{F}$, $\mathbf{G}$ represent the convective and $\mathbf{F_v}$, $\mathbf{G_v}$ the viscous fluxes in ξ- and η-direction, respectively. For the sake of compactness the generalized curvilinear coordinate ψ is introduced, allowing for a common formulation of the convective flux with

$$\mathbf{E}_\psi = \begin{pmatrix} \rho\,\theta_\psi \\ \rho u\,\theta_\psi + J\psi_x p \\ \rho v\,\theta_\psi + J\psi_y p \\ H\,\theta_\psi - J\psi_t p \end{pmatrix} . \qquad (3)$$

By substituting ψ with ξ or η, the convective fluxes in the individual directions are obtained, i.e. $\mathbf{F} = \mathbf{E}_\xi, \mathbf{G} = \mathbf{E}_\eta$. In analogy the generalized viscous flux vector becomes

$$\mathbf{E}_{\mathbf{v}\psi} = \begin{pmatrix} 0 \\ J\psi_x\tau_{xx} + J\psi_y\tau_{yx} \\ J\psi_x\tau_{xy} + J\psi_y\tau_{yy} \\ J\psi_x\Pi_x + J\psi_y\Pi_y \end{pmatrix} , \qquad (4)$$

with $\mathbf{F}_v = \mathbf{E}_{v\xi}$ and $\mathbf{G}_v = \mathbf{E}_{v\eta}$. In Eq. (3) θ_ψ substitutes for the generalized contravariant velocity modfied by J, while H represents the total enthalpy per unit volume:

$$\theta_\psi = J\psi_x u + J\psi_y v + J\psi_t , \quad H = \rho e + p . \qquad (5)$$

Furthermore p denotes the static pressure, considered the fifth primitive dependent variable. The components of the Cartesian shear stress tensor τ_{xx}, τ_{yy} and τ_{xy}=τ_{yx} appearing in Eq. (4) are given for a Newtonian fluid under consideration of Stoke's hypothesis by

$$\begin{aligned} \tau_{xx} &= \mu\left(\frac{4}{3}\frac{\partial u}{\partial x} - \frac{2}{3}\frac{\partial v}{\partial y}\right), \tau_{yy} = \mu\left(\frac{4}{3}\frac{\partial v}{\partial y} - \frac{2}{3}\frac{\partial u}{\partial x}\right), \\ \tau_{xy} &= \mu\left(\frac{\partial u}{\partial y} + \frac{\partial v}{\partial x}\right), \end{aligned} \qquad (6)$$

with μ being the molecular viscosity. Energy fluxes resulting from shear stress work and heat transfer are represented in Eq. (4) through

$$\Pi_x = u\tau_{xx} + v\tau_{xy} - q_x , \; \Pi_y = u\tau_{yx} + v\tau_{yy} - q_y . \qquad (7)$$

The elements of the Cartesian heat flux vector q_x and q_y obey Fourier's law of heat conduction:

$$q_x = \frac{-\gamma}{\gamma - 1}\frac{\mu}{Pr}\frac{\partial T}{\partial x} , \quad q_y = \frac{-\gamma}{\gamma - 1}\frac{\mu}{Pr}\frac{\partial T}{\partial y} . \qquad (8)$$

For air the ratio of specific heats γ is set to 1.4 and the Prandtl number Pr to 0.72. Assuming a calorically perfect gas, connectivity between the static temperature T and p is achieved through the thermal equation of state $T = p/\rho$. Supplemented by the caloric equation of state and the definition for e, an additional relationship between p and the conservative variables is derived:

$$p = (\gamma - 1)\left[\rho e - \frac{(\rho u)^2 + (\rho v)^2}{2\rho}\right] . \qquad (9)$$

Final closure of the the equation system is provided through Sutherland's law for the molecular viscosity, formulated in respect to aerodynamic flows as

$$\mu = \mu_\infty T^{\frac{3}{2}}\frac{1+S}{T+S} , \quad \text{with} \quad \mu_\infty = \sqrt{\gamma}\,\frac{Ma_\infty}{Re_\infty} l_{Re_\infty} . \qquad (10)$$

The Sutherland constant is defined by $S = 110\,[K]\,/\,T_\infty$, with T_∞ being the dimensional freestream static temperature in Kelvin. Compressible similarity to real flow conditions is realized per initialization of the freestream velocity with $u_\infty = \sqrt{\gamma}\,Ma_\infty$. The freestream Mach and Reynolds number, Ma_∞ and Re_∞ respectively, as well as the characteristic length l_{Re_∞} used in the formation of Re_∞, determine the freestream molecular viscosity μ_∞. Consequently, adjustment of μ_∞ through these parameters allows for viscous similarity.

In consideration of a finite volume approach for discretizing the Navier-Stokes equations on a structured grid, J appearing in Eq. (2) represents the volume of an individual cell, whereas the generalized metric terms $J\psi_x$ and $J\psi_y$ in Eq. (3-5) are the Cartesian components of the cell face normal vector for the ψ-direction. Additionally, $J\psi_t$ gives the time rate of change resulting from cell face movement for this vector. Specific definition of the metric terms is provided in [12]. Velocity and temperature gradients appearing in Eq. (6) and Eq. (8), respectively, are not subjected to the

curvilinear transformation, as a direct evaluation in the Cartesian coordinate system is numerically feasible.

2.2 Derivation and Linearization of the Perturbed Flow Governing Equations

2.2.1 *The Triple Decomposition*

Considering the periodic oscillation of an aerodynamic body under steady freestream conditions, the imposition of an organized unsteadiness onto the viscous flow field can be observed. In regard to the numerical simulation of this problem, the disturbance is mathematically introduced into the instantaneous Navier-Stokes equations Eq. (1) by way of the metric terms. Embedded in a computational grid, the body's movement corresponds to a dislocation of its discretized boundary, subsequently deforming the initial mesh. Therefore, it becomes possible to separate the motion of the spatial coordinate for each individual grid point into a steady mean and periodically perturbed component, distinguished by $\bar{}$ and $\tilde{}$ respectively:

$$\begin{aligned} x(\xi,\eta,\tau) &= \bar{x}(\xi,\eta)+\tilde{x}(\xi,\eta,\tau)\,, \\ y(\xi,\eta,\tau) &= \bar{y}(\xi,\eta)+\tilde{y}(\xi,\eta,\tau)\,. \end{aligned} \tag{11}$$

As J and the generalized metric terms $J\psi_{x,y,t}$ are directly calculated from the coordinates, they can be reformulated in a similar manner as

$$J = \bar{J}+\tilde{J}\,, \quad J\psi_{x,y,t} = \overline{J\psi}_{x,y,t}+\widetilde{J\psi}_{x,y,t}\,. \tag{12}$$

Due to the fact that the disturbance is externally imposed, the frequency of the unsteady turbulent flow's underlying organized oscillation is known. In the following the period of oscillation is identified by T. Postulating the negligibility of higher harmonics in the response, a triple decomposition of the flow development as suggested by Laschka [14] becomes feasible. An arbitrary instantaneous field quantity Φ is separated into a steady mean component $\bar{\Phi}$, a periodic perturbation $\tilde{\Phi}$ and a turbulent fluctuation Φ':

$$\begin{aligned} \Phi(\xi,\eta,\tau) &= \langle\Phi(\xi,\eta,\tau)\rangle+\Phi'(\xi,\eta,\tau) \\ &= \bar{\Phi}(\xi,\eta)+\tilde{\Phi}(\xi,\eta,\tau)+\Phi'(\xi,\eta,\tau) \end{aligned} \tag{13}$$

After substituting each individual primitive variable in the instantaneous Navier-Stokes equations Eq. (1) with their equivalent decomposed quantity according to Eq. (13), disjoined application of the phase average

$$\langle\Phi(\xi,\eta,\tau)\rangle = \lim_{N\to\infty}\frac{1}{N}\sum_{n=1}^{N}\Phi(\xi,\eta,\tau+n\cdot T) \tag{14}$$

and the time average

$$\bar{\Phi}(\xi,\eta) = \frac{1}{T}\int_{\tau}^{\tau+T}\Phi(\xi,\eta,\check{\tau})\,d\check{\tau} \tag{15}$$

yields two distinct sets of equations, governing unsteady and steady mean flow, respectively. In both cases the existent turbulent fluctuations are exclusively composited into averaged correlation terms, the necessary mathematical identities for this process having been provided by Telionis [24]. With the emergence of these turbulent correlations additional unknowns are introduced into the system, presenting a problem of closure that will require further handling. By subtracting the time averaged equation system from the phase averaged one, the governing equations for the periodic perturbed flow are obtained, or as formulated symbolically with the arbitrary flow quantity:

$$\tilde{\Phi}(\xi,\eta,\tau) = \langle\Phi(\xi,\eta,\tau)\rangle-\bar{\Phi}(\xi,\eta)\,. \tag{16}$$

2.2.2 *Treatment of Higher Order Perturbation Terms and Turbulent Correlations*

In order to demonstrate the technique described in 2.2.1 the convective flux in ξ-direction $\mathbf{F}=\mathbf{E}_{\xi}$ is selected. Reformulating the vector's second component F_2 as

$$\begin{aligned} F_2 &= J\xi_t(\rho u) + J\xi_x(\rho u^2+p) + J\xi_y(\rho uv) \\ &= F_{20} + F_{21} + F_{22}\,, \end{aligned} \tag{17}$$

the term F_{21} representing the transformed momentum in Cartesian x-direction is chosen for the specific analysis. Decomposing the metric and the primitive quantities constituting F_{21} in accordance with Eq. (12) and Eq. (13), while subsequently applying the phase average Eq. (14),

yields

$$\begin{aligned}\langle F_{21}\rangle &= (\overline{J\xi}_x + \widetilde{J\xi}_x)(\bar{\rho}\bar{u}^2 + 2\bar{\rho}\bar{u}\tilde{u} + 2\tilde{\rho}\tilde{u}\bar{u} \\ &+ \tilde{\rho}\bar{u}^2 + \bar{\rho}\tilde{u}^2 + \tilde{\rho}\tilde{u}^2 + \langle\langle\rho\rangle u'u'\rangle + \langle p\rangle)\,.\end{aligned} \tag{18}$$

In obtaining Eq. (18) the following considerations have been made: First, the density fluctuation ρ' has been omitted, as for non-hypersonic freestream Mach numbers and insignificant heat transfer the turbulence structure is similar to that of incompressible flows (Morkovin [16]). Second, simple mathematical identities [24] applied after the averaging process allow for the elimination of many correlation products between the mean, perturbed and turbulent quantities. Consequently, the influence of turbulence on the momentum is reduced to the single remaining averaged term $\langle\langle\rho\rangle u'u'\rangle$ identified as a component of the unsteady Reynolds stress tensor.

Under the assumption of small disturbances, i.e. the degree of unsteadiness imposed onto the flow leads to only minor variations of the mean steady state, higher order perturbation terms appearing in Eq. (18) are deemed negligible. In this regard, terms composited through multiple perturbed primitive quantities, e.g. $\overline{J\xi}_x 2\tilde{\rho}\tilde{u}\bar{u}$, as well as terms combining a perturbed metric with a perturbed primitive quantity, e.g. $\widetilde{J\xi}_x\tilde{\rho}\bar{u}^2$, are disregarded. This process marks a linearization in respect to the time-dependent quantities, indicated through an additional * when rewritting $\langle F_{21}\rangle$:

$$\begin{aligned}\langle F_{21}\rangle^* &= \overline{J\xi}_x(\bar{\rho}\bar{u}^2 + 2\bar{\rho}\bar{u}\tilde{u} + \tilde{\rho}\bar{u}^2 \\ &+ \langle\langle\rho\rangle u'u'\rangle + \langle p\rangle^*) \\ &+ \widetilde{J\xi}_x^*(\bar{\rho}\bar{u}^2 + \overline{\langle\rho\rangle u'u'} + \bar{p}^*)\,.\end{aligned} \tag{19}$$

Likewise, succesive deomposition, time averaging with Eq. (15) and linearization yields the steady mean part of term F_{21}:

$$\bar{F}^*_{21} = \overline{J\xi}_x(\bar{\rho}\bar{u}^2 + \overline{\langle\rho\rangle u'u'} + \bar{p}^*)\,. \tag{20}$$

In analogy $\overline{\langle\rho\rangle u'u'}$ is identified as a steady component of the Reynolds stress tensor. Furthermore, emerging linearized phase and time averages of the static pressure, $\langle p\rangle^*$ and $\bar{p}^*$ respectively, constitute additional unknowns. By subtracting Eq. (20) from Eq. (19) as per Eq. (16) the sought after linearized perturbation of term F_{21} is obtained to

$$\begin{aligned}\tilde{F}^*_{21} &= \langle F_{21}\rangle^* - \bar{F}^*_{21} \\ &= \overline{J\xi}_x(2\bar{\rho}\bar{u}\tilde{u} + \tilde{\rho}\bar{u}^2 + \tilde{p}^*) + \widetilde{J\xi}_x^*(\bar{\rho}\bar{u}^2 + \bar{p}^*) \\ &+ \overline{J\xi}_x\widetilde{\langle\rho\rangle u'u'} + \widetilde{J\xi}_x^*\overline{\langle\rho\rangle u'u'}\,,\end{aligned} \tag{21}$$

with $\tilde{p}^* = \langle p\rangle^* - \bar{p}^*$ being the equivalent formulation for the static pressure. The periodic pertubation of the Reynolds stress component is incorporated into Eqn. (21) through

$$\widetilde{\langle\rho\rangle u'u'} := \langle\langle\rho\rangle u'u'\rangle - \overline{\langle\rho\rangle u'u'}\,, \tag{22}$$

as defined by Acharaya [1] and Norris [17].

Localizing the viscous flux vector term corresponding to F_{21} in

$$F_{v2} = J\xi_x\tau_{xx} + J\xi_y\tau_{yx} = F_{v21} + F_{v22} \tag{23}$$

as F_{v21}, subsequent application of the triple decomposition and linearization results in

$$\tilde{F}^*_{v21} = \langle F_{v21}\rangle^* - \bar{F}^*_{v21} = \overline{J\xi}_x\tilde{\tau}^*_{xx} + \widetilde{J\xi}_x^*\bar{\tau}^*_{xx} \tag{24}$$

for the perturbation part. Through basic mathematical manipulation of the emerging perturbed flow governing equations the Reynolds stress terms isolated in Eq. (21) are extracted and introduced into Eq. (24). Alignment with the corresponding shear stress terms yields

$$\begin{aligned}\tilde{F}^*_{v21} &= \overline{J\xi}_x(\tilde{\tau}^*_{xx} - \widetilde{\langle\rho\rangle u'u'}) + \widetilde{J\xi}_x^*(\bar{\tau}^*_{xx} - \overline{\langle\rho\rangle u'u'}) \\ &= \overline{J\xi}_x\tilde{\tau}^*_{tot,xx} + \widetilde{J\xi}_x^*\bar{\tau}^*_{tot,xx}\quad,\end{aligned} \tag{25}$$

with $\tilde{\tau}^*_{tot,xx}$ and $\bar{\tau}^*_{tot,xx}$ representing the composited linearized perturbed and mean total shear stress, respectively. Extending Boussinesq's assumption to the perturbed flow analysis, the contribution of the Reynolds stress to the total shear stress is approximated through the perturbed and mean velocity gradients in conjunction with a decomposed eddy viscosity. The perturbed component being expressed as

$$\begin{aligned}\tilde{\tau}^*_{tot,xx} &= (\bar{\mu} + \bar{\mu}_t)\left(\frac{4}{3}\frac{\partial\tilde{u}}{\partial x} - \frac{2}{3}\frac{\partial\tilde{v}}{\partial y}\right) \\ &+ (\tilde{\mu}^* + \tilde{\mu}^*_t)\left(\frac{4}{3}\frac{\partial\bar{u}}{\partial x} - \frac{2}{3}\frac{\partial\bar{v}}{\partial y}\right),\end{aligned} \tag{26}$$

while the mean part retains the familiar formulation:

$$\overline{\tau}^*_{tot,xx} = (\overline{\mu}+\overline{\mu}_t)\left(\frac{4}{3}\frac{\partial \overline{u}}{\partial x} - \frac{2}{3}\frac{\partial \overline{v}}{\partial y}\right). \tag{27}$$

Consequently, the problem of closure in respect to the unknown Reynolds stresses is reduced to the modelling of the perturbed and mean eddy viscosities, $\tilde{\mu}^*_t$ and $\overline{\mu}_t$ respectively. Furthermore, a law governing the perturbed molecular viscosity $\tilde{\mu}^*$ has to be derived. The steady component $\overline{\mu}$ is obtained directly from Eq. (10) when inserting the mean static Temperature $\overline{T}^*$.

In this context, triple decomposition and linearization of the energy equation contained in Eq. (1) is far more complex than for the momentum equations. Undergoing the previously described process, a variety of turbulent energy correlation terms, such as Reynolds stress work and turbulent heat fluxes, have to be localized in the convective fluxes and appropriately incorporated into the viscous fluxes. Taking Π_x from Eq. (7), for example, we obtain

$$\tilde{\Pi}^*_x = \overline{u}\tilde{\tau}^*_{tot,xx} + \overline{v}\tilde{\tau}^*_{tot,xy} + \tilde{u}\overline{\tau}^*_{tot,xx} + \tilde{v}\overline{\tau}^*_{tot,xy} - \tilde{q}^*_{tot,x} \tag{28}$$

for the perturbed component, while the mean part yields

$$\overline{\Pi}^*_x = \overline{u}\overline{\tau}^*_{tot,xx} + \overline{v}\overline{\tau}^*_{tot,xy} - \overline{q}^*_{tot,x}. \tag{29}$$

Again falling back on Boussinesq, turbulent heat flux terms are accounted for in the composites $\tilde{q}^*_{tot,x}$ and $\overline{q}^*_{tot,x}$ through the perturbed and mean temperature gradients in conjunction with the decomposed eddy viscosity. Hence, the linearized perturbation of the total heat flux is governed by

$$\tilde{q}^*_{tot,x} = \frac{-\gamma}{\gamma-1}\left[\left(\frac{\overline{\mu}}{Pr}+\frac{\overline{\mu}_t}{Pr_t}\right)\frac{\partial \tilde{T}^*}{\partial x} + \left(\frac{\tilde{\mu}^*}{Pr}+\frac{\tilde{\mu}^*_t}{Pr_t}\right)\frac{\partial \overline{T}^*}{\partial x}\right], \tag{30}$$

with the steady counterpart formulated in familiar fashion as

$$\overline{q}^*_{tot,x} = \frac{-\gamma}{\gamma-1}\left(\frac{\overline{\mu}}{Pr}+\frac{\overline{\mu}_t}{Pr_t}\right)\frac{\partial \overline{T}^*}{\partial x}. \tag{31}$$

The newly introduced turbulent Prandtl number Pr_t is set to 0.9.

2.2.3 Time Domain Formulation

Consistent application of the triple decomposition to the instantaneous Navier-Stokes equations, while treating higher order terms and turbulent correlations, results in the linearized governing equations of the perturbed flow [18]. Casting the equations in a strong conservation form equivalent to Eq. (1) yields

$$\frac{\partial \tilde{\mathbf{Q}}^*}{\partial \tau} + \frac{\partial \tilde{\mathbf{F}}^*}{\partial \xi} + \frac{\partial \tilde{\mathbf{G}}^*}{\partial \eta} = \frac{\partial \tilde{\mathbf{F}}^*_{\mathbf{v}}}{\partial \xi} + \frac{\partial \tilde{\mathbf{G}}^*_{\mathbf{v}}}{\partial \eta}. \tag{32}$$

Time dependency is now restricted to the unknown perturbed quantities, which appear only in linear combinations with provided mean quantities throughout the equation system. In this regard the transformed state vector $\tilde{\mathbf{Q}}^*$ decomposes into

$$\tilde{\mathbf{Q}}^* = \bar{J}\tilde{\mathbf{q}}^* + \tilde{J}^*\overline{\mathbf{q}}^*, \tag{33}$$

the linearized Cartesian vectors of the perturbed and mean conservative variables, $\tilde{\mathbf{q}}^*$ and $\overline{\mathbf{q}}^*$ respectively, being

$$\tilde{\mathbf{q}}^* = \left(\tilde{\rho}, \widetilde{\rho u}^*, \widetilde{\rho v}^*, \widetilde{\rho e}^*\right)^T, \quad \overline{\mathbf{q}}^* = \left(\overline{\rho}, \overline{\rho u}^*, \overline{\rho v}^*, \overline{\rho e}^*\right)^T. \tag{34}$$

With the exception of density, elements appearing in Eq. (34) are defined by use of perturbed and mean primitive variables, e.g. the momentum in Cartesian x-direction is given by

$$\widetilde{\rho u}^* := \overline{\rho}\tilde{u} + \tilde{\rho}\overline{u}, \quad \overline{\rho u}^* := \overline{\rho}\overline{u}. \tag{35}$$

2.3 Closing the Equation System

2.3.1 Pressure

Applying the techniques from 2.2.1 and 2.2.2 to the thermal equation of state, connectivity between the perturbed static temperature $\tilde{T}^*$ and pressure $\tilde{p}^*$ is achieved per $\tilde{T}^* = (\tilde{p}^* - \tilde{\rho}\overline{T}^*)/\overline{\rho}$ supplemented by $\overline{T}^* = \overline{p}^*/\overline{\rho}$. In analogy, formulations for $\tilde{p}^*$ and $\overline{p}^*$ as functions of the decomposed conservative variables are obtained through Eq. (9). Disregrading turbulent kinetic energy terms emerging from the averaging process, the linearized law governing $\tilde{p}^*$ becomes equivalent to the one used for closing the

small disturbance Euler equations [12]. Likewise, $\bar{p}^*$ results directly from inserting the linearized mean conservative variables composing $\bar{\mathbf{q}}^*$ into Eq. (9).

2.3.2 Molecular Viscosity

As Sutherland's law defies standard decomposition into a perturbed and mean part due to its mathematical nature, an alternative approach based on a first order Taylor series expansion of Eq. (10) about the mean static temperature is pursued. Consequently, the perturbed molecular viscosity $\tilde{\mu}^*$ is calculated from $\tilde{T}^*$ with

$$\tilde{\mu}^* = \left.\frac{\partial \mu}{\partial T}\right|_{\bar{T}^*} \cdot \tilde{T}^* = \frac{\bar{\mu}}{\bar{T}^* + S}\left[\frac{3(\bar{T}^* + S)}{2\bar{T}^*} - 1\right] \cdot \tilde{T}^*, \tag{36}$$

satisfying the small disturbance consideration.

2.3.3 Eddy Viscosity

In the present study the Spalart-Allmaras turbulence model [23] is employed for calculating the perturbed as well as the mean eddy viscosity throughout the flow field. Constructed as one additional partial differential equation its incorporation into the existing equation system is not only straightforward, but more importantly lends itself to complete linearization [6]. As the model's auxiliary functions (f_{v1}, f_{v2}, f_w) are all continuosly differentiable, a Taylor series expansion becomes feasible, when standard decomposition fails. The basic turbulence model accounts for convection, diffusion, production and destruction of the eddy viscosity μ_t as formulated in terms of the conservative working variable $\breve{\mu} := \rho\breve{\nu}$, with $\breve{\nu}$ being its primitive counterpart. The relationship between μ_t and $\breve{\mu}$ is given through

$$\mu_t = \breve{\mu}\, f_{v1}, \quad \text{with} \quad f_{v1} = \frac{\chi^3}{\chi^3 + c_{v1}^3} \quad \text{and} \quad \chi := \frac{\breve{\mu}}{\mu}. \tag{37}$$

Written in strong conservation form for curvilinear coordinates the equation governing $\breve{\mu}$ becomes formally similiar to Eq. (1) and therefore is easily included into the Navier-Stokes equation system as

$$\frac{\partial Q_5}{\partial \tau} + \frac{\partial F_5}{\partial \xi} + \frac{\partial G_5}{\partial \eta} = \frac{\partial F_{v5}}{\partial \xi} + \frac{\partial G_{v5}}{\partial \eta} + T_5. \tag{38}$$

The fifth components of the solution vector, the generalized convective and viscous flux vectors, $\mathbf{Q}$, $\mathbf{E}_\psi$ and $\mathbf{E}_{\mathbf{v}\psi}$ respectively, being specified to

$$Q_5 = J\breve{\mu}, \quad E_{5\psi} = \breve{\mu}\theta_\psi, \quad E_{v5\psi} = J\psi_x \tau_{\breve{\mu}x} + J\psi_y \tau_{\breve{\mu}y}. \tag{39}$$

The viscous flux component $E_{v5\psi}$ is constructed to allow for second order diffusion in respect to $\breve{\mu}$, with the appearing viscous shear stress equivalent terms $\tau_{\breve{\mu}x}$ and $\tau_{\breve{\mu}y}$ defined through

$$\tau_{\breve{\mu}x} = \frac{\mu + \breve{\mu}}{\sigma}\frac{\partial}{\partial x}\left(\frac{\breve{\mu}}{\rho}\right), \; \tau_{\breve{\mu}y} = \frac{\mu + \breve{\mu}}{\sigma}\frac{\partial}{\partial y}\left(\frac{\breve{\mu}}{\rho}\right). \tag{40}$$

Turbulent production $P_{\breve{\mu}}$, destruction $D_{\breve{\mu}}$ and first order diffusion $F_{\breve{\mu}}$ are composited into the source term

$$T_5 = J\left(P_{\breve{\mu}} + D_{\breve{\mu}} + F_{\breve{\mu}}\right), \tag{41}$$

with production being governed by

$$P_{\breve{\mu}} = c_{b1}|\breve{\omega}|\breve{\mu} \quad \text{and} \quad |\breve{\omega}| = |\omega| + \frac{\breve{\mu}}{\rho\kappa^2 d^2} f_{v2}. \tag{42}$$

In Eq. (42) d represents the distance of the considered field point to the nearest wall, $|\omega|$ substitutes for the magnitude of vorticity, while f_{v2} provides near wall dampening:

$$|\omega| = \left|\frac{\partial v}{\partial x} - \frac{\partial u}{\partial y}\right|, \quad f_{v2} = 1 - \frac{\chi}{1 + \chi\, f_{v1}}. \tag{43}$$

Furthermore, turbulent destruction is considered through

$$D_{\breve{\mu}} = -\frac{c_{wl}\, f_w}{\rho}\left(\frac{\breve{\mu}}{d}\right)^2 \quad \text{and} \quad f_w = g\left(\frac{1 + c_{w3}^6}{g^6 + c_{w3}^6}\right)^{\frac{1}{6}}, \tag{44}$$

with the auxiliary expressions

$$g = r + c_{w2}(r^6 - r) \quad \text{and} \quad r = \frac{\breve{\mu}}{\rho|\breve{\omega}|\kappa^2 d^2}. \tag{45}$$

Utilizing the nabla operator $\vec{\nabla}$, first order diffusion is expressed compactly as

$$F_{\breve{\mu}} = \frac{\rho c_{b2}}{\sigma}\left[\vec{\nabla}\left(\frac{\breve{\mu}}{\rho}\right)\right]^2. \tag{46}$$

The calibration constants c_{v1}, σ, c_{b1}, c_{b2}, κ, c_{w1}, c_{w2} and c_{w3} appearing in Eq. (37-46) are given in [23]. Only fully turbulent flow is considered

in this context, i.e. no modelling of transition is contained in the previous equations.

Consistent application of the discussed linearization techniques to the Spalart-Allmaras turbulence model yields a small disturbance formulation for the equations governing the perturbed eddy viscosity $\tilde{\mu}_t^*$. In analogy $\tilde{\mu}_t^*$ is dependent on the perturbed as well as the mean component of the working variable, $\widetilde{\breve{\mu}}^*$ and $\bar{\breve{\mu}}$ respectively. Conforming with Eq. (35), $\widetilde{\breve{\mu}}^*$ itself decomposes into linear terms of its perturbed and mean primitive quantities $\widetilde{\breve{\mu}}^* := \bar{\breve{\rho}}\tilde{\breve{\nu}} + \tilde{\breve{\rho}}\bar{\breve{\nu}}$ Accordingly, $\tilde{\mu}_t^*$ is expressed through

$$\tilde{\mu}_t^* = \bar{\breve{\mu}}\,\tilde{f}_{v1}^* + \widetilde{\breve{\mu}}^*\,\bar{f}_{v1}\,, \text{ with } \tilde{f}_{v1}^* = \frac{3\bar{\chi}^2 c_{v1}^3}{(\bar{\chi}^3 + c_{v1}^3)^2}\,\tilde{\chi}^* \quad (47)$$

$$\text{and} \quad \tilde{\chi}^* := \bar{\mu}^{-2}(\bar{\mu}\widetilde{\breve{\mu}}^* - \widetilde{\mu}^*\bar{\breve{\mu}})\,. \quad (48)$$

As becomes evident in Eq. (47), mean values of functions or supplemental quantities associated with the Spalart-Allmaras turbulence model will appear throughout the following linearized equations. Denoted by $\bar{}$, they are obtained directly when expressing Eq. (37-46) for the steady state, i.e. the formulation required when calculating $\bar{\mu}_t$.

The strong conservation form of Eq. (38) is retained by the equation governing $\widetilde{\breve{\mu}}^*$

$$\frac{\partial \tilde{Q}_5^*}{\partial\tau} + \frac{\partial \tilde{F}_5^*}{\partial\xi} + \frac{\partial \tilde{G}_5^*}{\partial\eta} = \frac{\partial \tilde{F}_{v5}^*}{\partial\xi} + \frac{\partial \tilde{G}_{v5}^*}{\partial\eta} + \tilde{T}_5^*\,, \quad (49)$$

allowing its incorporation into the linearized perturbed flow equation system Eq. (32). The fifth component of the perturbed solution vector $\tilde{\mathbf{Q}}^*$ and generalized convective flux $\tilde{\mathbf{E}}_\psi^*$ are derived as

$$\tilde{Q}_5^* = \bar{J}\,\widetilde{\breve{\mu}}^* + \tilde{J}^*\,\bar{\breve{\mu}}, \quad \tilde{E}_{5\psi}^* = \bar{\breve{\mu}}\tilde{\theta}_\psi^{(1)} + \bar{\breve{\mu}}\tilde{\theta}_\psi^{(2)} + \widetilde{\breve{\mu}}^*\,\bar{\theta}_\psi\,, \quad (50)$$

respectively. Through the decomposition three variants of the modified generalized contravariant velocity θ_ψ arise in $\tilde{E}_{5\psi}^*$:

$$\begin{aligned} \tilde{\theta}_\psi^{(1)} &= \overline{J\psi_x}\tilde{u} + \overline{J\psi_y}\tilde{v}, \quad \bar{\theta}_\psi = \overline{J\psi_x}\bar{u} + \overline{J\psi_y}\bar{v} \\ \tilde{\theta}_\psi^{(2)} &= \widetilde{J\psi_x}^*\bar{u} + \widetilde{J\psi_y}^*\bar{v} + \widetilde{J\psi_t}^*\,. \end{aligned} \quad (51)$$

On one hand $\tilde{\theta}_\psi^{(1)}$ contains only combinations of the perturbed velocities with the mean metrics, while on the other $\tilde{\theta}_\psi^{(2)}$ is composited by mean velocities and the perturbed metrics, i.e. complimentary to $\tilde{\theta}_\psi^{(1)}$. $\bar{\theta}_\psi$ being the mean state of Eq. (5). Likewise, the fifth component of the generalized viscous flux $\tilde{\mathbf{E}}_{v\psi}^*$ separates into

$$\tilde{E}_{v5\psi}^* = \overline{J\psi_x}\tilde{\tau}_{\breve{\mu}x}^* + \overline{J\psi_y}\tilde{\tau}_{\breve{\mu}y}^* + \widetilde{J\psi_x}^*\bar{\tau}_{\breve{\mu}x} + \widetilde{J\psi_y}^*\bar{\tau}_{\breve{\mu}y}, \quad (52)$$

with $\tilde{\tau}_{\breve{\mu}x}^*$ and $\tilde{\tau}_{\breve{\mu}y}^*$ representing the perturbed parts of the viscous shear stress equivalent terms, e.g.

$$\tilde{\tau}_{\breve{\mu}x}^* = \frac{\bar{\mu}+\bar{\breve{\mu}}}{\sigma}\frac{\partial}{\partial x}\left(\frac{\widetilde{\breve{\mu}}^*}{\bar{\rho}} - \bar{\breve{\mu}}\frac{\tilde{\rho}^*}{\bar{\rho}^2}\right) + \frac{\tilde{\mu}+\widetilde{\breve{\mu}}^*}{\bar{\mu}+\bar{\breve{\mu}}}\,\bar{\tau}_{\breve{\mu}x}. \quad (53)$$

$\tilde{\tau}_{\breve{\mu}y}^*$ is obtained directly by substituting the partial derivative $\partial/\partial x$ in Eq. (53) with $\partial/\partial y$ and $\bar{\tau}_{\breve{\mu}x}$ with $\bar{\tau}_{\breve{\mu}y}$. Continuing in similar manner, the perturbation of the turbulent source term is expressed through

$$\tilde{T}_5^* = \bar{J}(\tilde{P}_{\breve{\mu}}^* + \tilde{D}_{\breve{\mu}}^* + \tilde{F}_{\breve{\mu}}^*) + \tilde{J}^*(\bar{P}_{\breve{\mu}} + \bar{D}_{\breve{\mu}} + \bar{F}_{\breve{\mu}}), \quad (54)$$

with production being governed by the following set of equations:

$$\tilde{P}_{\breve{\mu}}^* = \bar{P}_{\breve{\mu}}\cdot\left(\frac{\widetilde{\breve{\mu}}^*}{\bar{\breve{\mu}}} + \frac{\widetilde{|\breve{\omega}|}^*}{\overline{|\breve{\omega}|}}\right), \quad \Delta\overline{|\omega|} = \overline{|\breve{\omega}|} - \overline{|\omega|}, \quad (55)$$

$$\widetilde{|\breve{\omega}|}^* = \widetilde{|\omega|}^* + \Delta\overline{|\omega|}\left(\frac{\tilde{f}_{v2}^*}{\bar{f}_{v2}} + \frac{\widetilde{\breve{\mu}}^*}{\bar{\breve{\mu}}} - \frac{\tilde{\rho}}{\bar{\rho}} - 2\frac{\tilde{d}}{\bar{d}}\right). \quad (56)$$

Eq. (56) utilizes linearized formulations of the magnitude of vorticity and the near wall dampening function, derived as

$$\widetilde{|\omega|}^* = \overline{|\omega|}^{-1}\left(\frac{\partial\bar{v}}{\partial x} - \frac{\partial\bar{u}}{\partial y}\right)\left(\frac{\partial\tilde{v}}{\partial x} - \frac{\partial\tilde{u}}{\partial y}\right) \quad (57)$$

$$\text{and} \quad \tilde{f}_{v2}^* = \frac{\tilde{f}_{v1}^*\bar{\chi}^2 - \tilde{\chi}^*}{(1+\bar{f}_{v1}\bar{\chi})^2}\,, \quad (58)$$

respectively. Furthermore, perturbed tubulent destruction obeys

$$\tilde{D}_{\breve{\mu}}^* = \bar{D}_{\breve{\mu}}\cdot\left(\frac{\tilde{f}_w^*}{\bar{f}_w} + 2\frac{\widetilde{\breve{\mu}}^*}{\bar{\breve{\mu}}} - \frac{\tilde{\rho}}{\bar{\rho}} - 2\frac{\tilde{d}}{\bar{d}}\right) \quad (59)$$

$$\text{and} \quad \tilde{f}_w^* = \frac{\bar{f}_w}{\bar{g}}\left(\frac{c_{w3}^6}{\bar{g}^6 + c_{w3}^6}\right)\tilde{g}^*\,, \quad (60)$$

with the auxiliary expressions

$$\tilde{g}^* = \left[1 + c_{w2}(6\bar{r}^5 - 1)\right] \tilde{r}^* \tag{61}$$

$$\text{and} \quad \tilde{r}^* = \bar{r}\left(\frac{\widetilde{\breve{\mu}}^*}{\bar{\breve{\mu}}} - \frac{\tilde{\rho}}{\bar{\rho}} - \frac{\widetilde{|\breve{\omega}|}^*}{\bar{|\breve{\omega}|}} - 2\frac{\tilde{d}}{\bar{d}}\right). \tag{62}$$

Finally, the linearized formulation of the first order diffusion term yields

$$\tilde{F}^*_{\breve{\mu}} = \frac{2\bar{\rho}c_{b2}}{\sigma}\vec{\nabla}\left(\frac{\bar{\breve{\mu}}}{\bar{\rho}}\right)\left[\vec{\nabla}\left(\frac{\widetilde{\breve{\mu}}^*}{\bar{\rho}}\right) - \vec{\nabla}\left(\frac{\bar{\breve{\mu}}\tilde{\rho}}{\bar{\rho}^2}\right)\right] + \frac{\tilde{\rho}}{\bar{\rho}}\bar{F}_{\breve{\mu}}. \tag{63}$$

2.4 The Small Disturbance Navier-Stokes Equations

Having provided closure in 2.3 and subsequently incorporating the turbulence model into Eq. (32), the linearized perturbed flow equation is subject to slight rearrangement in preparation of a frequency domain formulation.

As has become evident, for example in Eq. (51), decomposition and linearization yielded two basic sets of terms throughout the equation system: The first group, to be denoted by $^{(1)}$, exclusively contains the unknown perturbed flow quantities appearing in linear combination with mean flow quantities or metrics, i.e. they are homogenous in the perturbed solution vector $\tilde{\mathbf{q}}^*$. The complementary second group, hence distinguished by $^{(2)}$, solely consists of the perturbed metrics in linear combination with the mean flow quantities. All terms collected in group $^{(2)}$ are designated as known, because of the following considerations: The deformation of the computational grid is prescribed through the body's periodic motion, consequently supplying the perturbed metrics. Similar, the mean flow quantities can be provided in advance by a steady state Reynolds-averaged Navier-Stokes solution for the body's mean, i.e. reference, position. Hence, reformulation of the linearized perturbed flow equations as detailed in [20] isolates the $^{(2)}$ denoted vector components on the right hand side of the equation system:

$$\begin{aligned}\frac{\partial\tilde{\mathbf{Q}}^{(1)}}{\partial\tau} + \frac{\partial(\tilde{\mathbf{F}}^{(1)} - \tilde{\mathbf{F}}^{(1)}_{\mathbf{v}})}{\partial\xi}) + \frac{\partial(\tilde{\mathbf{G}}^{(1)} - \tilde{\mathbf{G}}^{(1)}_{\mathbf{v}})}{\partial\eta} = \\ -\left[\frac{\partial\tilde{\mathbf{Q}}^{(2)}}{\partial\tau} + \frac{\partial(\tilde{\mathbf{F}}^{(2)} - \tilde{\mathbf{F}}^{(2)}_{\mathbf{v}})}{\partial\xi} + \frac{\partial(\tilde{\mathbf{G}}^{(2)} - \tilde{\mathbf{G}}^{(2)}_{\mathbf{v}})}{\partial\eta}\right] \\ +\tilde{\mathbf{T}}^{(1)} + \tilde{\mathbf{T}}^{(2)}.\end{aligned} \tag{64}$$

It is obvious from Eq. (64), that the $^{(2)}$ components are exclusively reponsible for initiating the development of the perturbed solution and therefore are considered as the equation system's source terms.

Restriction of the body's motion to a harmonic oscillation allows the perturbed coordinates of the grid deformation to be expressed as

$$\tilde{x}(\xi,\eta,\tau) = \hat{x}(\xi,\eta)\cdot e^{ik\tau}, \quad \tilde{y}(\xi,\eta,\tau) = \hat{y}(\xi,\eta)\cdot e^{ik\tau}, \tag{65}$$

having been decomposed into a time invariant amplitude distinguished by $\hat{}$ and the respective complex time law $e^{ik\tau}$. In this context, i represents the imaginary unit and k the known non-dimensional frequency of the prescribed motion. As a consequence, the linearized perturbed cell volume and metrics result in

$$\tilde{J}^* = \hat{J}^*\cdot e^{ik\tau}, \quad \widetilde{J\psi}^*_{x,y,t} = \widehat{J\psi}^*_{x,y,t}\cdot e^{ik\tau}, \tag{66}$$

respectively. In order to avoid double notation, from this point on * will be dropped in connection with $\hat{}$ as the indicator of linearity. Modelling of the flow response occurs in similar manner: The perturbation of an arbitrary field quantity is defined as

$$\tilde{\Phi}(\xi,\eta,\tau) = \hat{\Phi}(\xi,\eta)\cdot e^{ik\tau}, \tag{67}$$

with $\hat{\Phi}$ representing the quantity's complex amplitude. Expressing each individual primitive perturbation variable appearing in Eq. (64) according to Eq. (67), results in a corresponding separation for the homogenous vector components:

$$\begin{aligned}\tilde{\mathbf{Q}}^{(1)} &= \hat{\mathbf{Q}}^{(1)}\cdot e^{ik\tau}, \quad \tilde{\mathbf{T}}^{(1)} = \hat{\mathbf{T}}^{(1)}\cdot e^{ik\tau}, \\ \tilde{\mathbf{E}}^{(1)}_{\psi} &= \hat{\mathbf{E}}^{(1)}_{\psi}\cdot e^{ik\tau}, \quad \tilde{\mathbf{E}}^{(1)}_{v\psi} = \hat{\mathbf{E}}^{(1)}_{v\psi}\cdot e^{ik\tau}.\end{aligned} \tag{68}$$

Likewise, $\tilde{J}^*$ and $\widetilde{J\psi}^*_{x,y,t}$ contained in the $^{(2)}$ vector components of Eq. (64) are replaced with Eq.

(66). As the time law $e^{ik\tau}$ now appears linearily in all components of the equation system, it can be eliminated completely. Thus, a formulation for the time invariant amplitude quantities of the flow perturbation is obtained. Recasting the governing equations for the complex amplitude of the state vector, i.e.

$$\hat{\mathbf{Q}}^{(1)} = \bar{J}\hat{\mathbf{q}} = \bar{J}\left(\hat{\rho}, \widehat{\rho u}, \widehat{\rho v}, \widehat{\rho e}, \hat{\breve{\mu}}\right)^T , \tag{69}$$

ultimately yields the small disturbance Navier-Stokes equations:

$$\frac{\partial \hat{\mathbf{Q}}^{(1)}}{\partial \tau} + \frac{\partial(\hat{\mathbf{F}}^{(1)} - \hat{\mathbf{F}}_{\mathbf{v}}^{(1)})}{\partial \xi} + \frac{\partial(\hat{\mathbf{G}}^{(1)} - \hat{\mathbf{G}}_{\mathbf{v}}^{(1)})}{\partial \eta} = \hat{\mathbf{S}}^{(1)} + \hat{\mathbf{S}}^{(2)} \tag{70}$$

The newly introduced source components $\hat{\mathbf{S}}^{(1)}$ and $\hat{\mathbf{S}}^{(2)}$ substitute for

$$\hat{\mathbf{S}}^{(1)} = -ik\hat{\mathbf{Q}}^{(1)} + \hat{\mathbf{T}}^{(1)}, \tag{71}$$

$$\hat{\mathbf{S}}^{(2)} = -\left[ik\hat{\mathbf{Q}}^{(2)} + \frac{\partial(\hat{\mathbf{F}}^{(2)} - \hat{\mathbf{F}}_{\mathbf{v}}^{(2)})}{\partial \xi} + \frac{\partial(\hat{\mathbf{G}}^{(2)} - \hat{\mathbf{G}}_{\mathbf{v}}^{(2)})}{\partial \eta} \right] + \hat{\mathbf{T}}^{(2)}. \tag{72}$$

Furthermore, the homogenous convective flux vectors are obtained directly through the generalized mean jacobian matrix $\bar{\mathbf{K}}_\psi$ multiplied by the Cartesian amplitude state vector $\hat{\mathbf{q}}$:

$$\hat{\mathbf{E}}_\psi^{(1)} = \left.\frac{\partial \mathbf{E}_\psi}{\partial \mathbf{q}}\right|_{\bar{\mathbf{q}}} \cdot \hat{\mathbf{q}} = \bar{\mathbf{K}}_\psi \cdot \hat{\mathbf{q}}, \tag{73}$$

$$\bar{\mathbf{K}}_\psi = \begin{pmatrix} 0 & \overline{J\psi}_x & \overline{J\psi}_y & 0 & 0 \\ \overline{J\psi}_x\bar{\phi} - \bar{u}\bar{\theta}_\psi & \bar{\theta}_\psi + (2-\gamma)\overline{J\psi}_x\bar{u} & \overline{J\psi}_y\bar{u} - (\gamma-1)\overline{J\psi}_x\bar{v} & (\gamma-1)\overline{J\psi}_x & 0 \\ \overline{J\psi}_y\bar{\phi} - \bar{v}\bar{\theta}_\psi & \overline{J\psi}_x\bar{v} - (\gamma-1)\overline{J\psi}_y\bar{u} & \bar{\theta}_\psi + (2-\gamma)\overline{J\psi}_y\bar{v} & (\gamma-1)\overline{J\psi}_y & 0 \\ (2\bar{\phi} - \gamma\bar{e})\bar{\theta}_\psi & (\gamma\bar{e} - \bar{\phi})\overline{J\psi}_x - (\gamma-1)\bar{\theta}_\psi\bar{u} & (\gamma\bar{e} - \bar{\phi})\overline{J\psi}_y - (\gamma-1)\bar{\theta}_\psi\bar{v} & \gamma\bar{\theta}_\psi & 0 \\ -\bar{\breve{\mu}}/\bar{\rho}\bar{\theta}_\psi & \bar{\breve{\mu}}/\bar{\rho}\overline{J\psi}_x & \bar{\breve{\mu}}/\bar{\rho}\overline{J\psi}_y & 0 & \bar{\theta}_\psi \end{pmatrix} \tag{74}$$

with

$$\bar{\theta}_\psi = \overline{J\psi}_x\bar{u} + \overline{J\psi}_y\bar{v}, \quad \bar{\phi} = [(\gamma-1)/2](\bar{u}^2 + \bar{v}^2). \tag{75}$$

The homogenous viscous flux and the turbulent source term vectors result in

$$\hat{\mathbf{E}}_{\mathbf{v}\psi}^{(1)} = \begin{pmatrix} 0 \\ \overline{J\psi}_x\hat{\tau}_{xx} + \overline{J\psi}_y\hat{\tau}_{yx} \\ \overline{J\psi}_x\hat{\tau}_{xy} + \overline{J\psi}_y\hat{\tau}_{yy} \\ \overline{J\psi}_x\hat{\Pi}_x + \overline{J\psi}_y\hat{\Pi}_y \\ \overline{J\psi}_x\hat{\tau}_{\breve{\mu}x} + \overline{J\psi}_y\hat{\tau}_{\breve{\mu}y} \end{pmatrix}, \tag{76}$$

$$\hat{\mathbf{T}}^{(1)} = \bar{J}\left(0, 0, 0, 0, \hat{P}_{\breve{\mu}} + \hat{D}_{\breve{\mu}} + \hat{F}_{\breve{\mu}}\right)^T , \tag{77}$$

respectively. Amplitude terms contained in Eq. (76-77), e.g. $\hat{\tau}_{xx}$, $\hat{\Pi}_x$, $\hat{\tau}_{\breve{\mu}x}$ or $\hat{P}_{\breve{\mu}}$, are expressed through the respective perturbed formulations derived in 2.2.2 and 2.3 by replacing the $\tilde{}$ identifier with $\hat{}$. Let it be noted, that for the sake of clarity the index $_{tot}$ has been dropped from the viscous shear stress and energy flux terms. Finally, the vector components compositing $\hat{\mathbf{S}}^{(2)}$ yield

$$\hat{\mathbf{Q}}^{(2)} = \hat{J}\bar{\mathbf{q}} = \hat{J}\left(\bar{\rho}, \overline{\rho u}, \overline{\rho v}, \overline{\rho e}, \bar{\breve{\mu}}\right)^T , \tag{78}$$

$$\hat{\mathbf{E}}_\psi^{(2)} = \begin{pmatrix} \bar{\rho}\hat{\theta}_\psi^{(2)} \\ \overline{\rho u}\hat{\theta}_\psi^{(2)} + \widehat{J\psi}_x\bar{p} \\ \overline{\rho v}\hat{\theta}_\psi^{(2)} + \widehat{J\psi}_y\bar{p} \\ \bar{H}\hat{\theta}_\psi^{(2)} - \widehat{J\psi}_t\bar{p} \\ \bar{\breve{\mu}}\hat{\theta}_\psi^{(2)} \end{pmatrix} \tag{79}$$

$$\text{with} \quad \hat{\theta}_\psi^{(2)} = \widehat{J\psi}_x\bar{u} + \widehat{J\psi}_y\bar{v} + \widehat{J\psi}_t, \tag{80}$$

$$\hat{\mathbf{E}}_{\mathbf{v}\psi}^{(2)} = \begin{pmatrix} 0 \\ \widehat{J\psi}_x\bar{\tau}_{xx} + \widehat{J\psi}_y\bar{\tau}_{yx} \\ \widehat{J\psi}_x\bar{\tau}_{xy} + \widehat{J\psi}_y\bar{\tau}_{yy} \\ \widehat{J\psi}_x\bar{\Pi}_x + \widehat{J\psi}_y\bar{\Pi}_y \\ \widehat{J\psi}_x\bar{\tau}_{\breve{\mu}x} + \widehat{J\psi}_y\bar{\tau}_{\breve{\mu}y} \end{pmatrix}, \tag{81}$$

$$\text{and} \quad \hat{\mathbf{T}}^{(2)} = \hat{J}(0, 0, 0, 0, \bar{P}_{\breve{\mu}} + \bar{F}_{\breve{\mu}} + \bar{D}_{\breve{\mu}})^T . \tag{82}$$

With the derivation of the small disturbance Navier-Stokes equations the initial unsteady problem has been reduced to a steady one for the complex amplitude flow quantities. As $\hat{\mathbf{Q}}^{(1)}$ is invariant to time, the derivative $\frac{\partial \hat{\mathbf{Q}}^{(1)}}{\partial \tau}$ consequently would vanish from Eq. (70). However, it is retained in the formulation in order to construct a pseudo-time marching solution scheme, thus artifically preserving the equation system's time hyberbolic mathematical nature. Coupling between the inphase (real) and out of phase (imaginary) parts of the complex equation system is provided by $ik\hat{\mathbf{Q}}^{(1)}$. For $k = 0$, i.e. the quasi-steady case, this interaction is eliminated, therefore restricting the solution to the real part. Letting $Re_\infty \rightarrow \infty$, while disregarding the turbulence model incorporated into Eq. (70), yields the small disturbance Euler equations as given in [12]. Thus, implementing the small disturbance Navier-Stokes method FLM-SD.NS on basis of the existing small disturbance Euler solver FLM-SDEu becomes reasonable. The definitions for the linearized amplitude volume $\hat{J}$ and metrics $\widehat{J\psi}_{x,y,t}$ appearing throughout Eq. (78-82) is also taken from [12].

3 Numerical Method

3.1 Properties

The numerical algorithm for solving Eq. (70) is constructed by incorporating the derived viscous and turbulence modelling components into the FLM-SDEu code. In this way the TVD property and Roe's convective flux difference splitting of the inviscid finite volume approach, as detailed in [12], are retained. Furthermore, with the introduction of the viscous fluxes and turbulence source term, Cartesian gradients of the primitive mean and amplitude quantities now have to be treated as well. For evaluation of these first-derivatives Chakravarthy's application of Gauss's integral theorem in high resolution schemes is employed [5]. The mean gradients are calculated through the basic method, while the assessment of the amplitude gradients occurs with a corresponding small disturbance formulation as detailed in [10]. Replacing the original explicit Runga-Kutta time-stepping scheme with an implict lower-upper symmetric successive overrelaxation (LU-SSOR) approach embedded in a multi-grid algorithm enhances the performance of the solution process. Efficient coupling of the LU-SSOR scheme with a multigrid technique has been initially proposed and investigated by Blazek [4] for the steady state Navier-Stokes equations. Retaining the properities of LU-SSOR, which is characterized by a diagonally dominant factorization, a corresponding small disturbance formulation for solving Eq. (70) has been developed and implemented [19]. Consistent treatment of the adiabatic wall and no-slip boundary condition [10] and their discrete realization completes the extension of FLM-SDEu to FLM-SD.NS.

In developing FLM-SD.NS special care has been taken in order to maintain numerical equivalency with the time-accurate Reynolds-averaged Navier-Stokes solver FLM-NS [7], which has recently been updated with the Spalart-Allmaras turbulence model and the multi-grid technique. As FLM-NS features the original non-linearized formulations of the discretization and integration schemes implemented in FLM-SD.NS, comparability between the time-accurate, i.e. non-linear, and small disturbance method exists.

3.2 Simulation Process

In a first step two computational grids are supplied: one for the reference position of the body and the other for the deflected extremum position, generated through deformation. A turbulent steady state solution then is produced with FLM-NS in the reference grid. It serves as input to FLM-SD.NS, providing the prerequisite mean flow values as contained in the source term $\hat{\mathbf{S}}^{(2)}$ and the convective flux jacobian $\bar{\mathbf{K}}_\psi$, Eq. (72) and Eq. (74) respectively. Furthermore, subtraction of the reference from the extremum grid by FLM-SD.NS during procedure initialization yields the amplitudes of the vertecies' coordinates, consequently supplying the required amplitude volume $\hat{J}$ and metrics $\widehat{J\psi}_{x,y,t}$. The components $\hat{\mathbf{S}}^{(2)}$ and

$\bar{\mathbf{K}}_\psi$ are calculated only once at the beginning of the procedure and kept in storage, as they remain invariant throughout the psuedo-time integration process. With FLM-SD.NS the first harmonic of the unsteady flow solution is obtained directly in form of the amplitude state vector's real- and imaginary part.

In contrast FLM-NS only uses the steady state solution for initialization of the non-linear unsteady computation, which is performed through conventional dual time-stepping. The required mesh movement is realized by interpolating intermediary grids between the extremum and reference position according to the time law, i.e. Eq. (11) with Eq. (65). Consequently, the complete unsteady solution evolves in the time domain, requiring a Fourier analysis in post processing for the extraction of the first harmonics.

4 Computational Results

4.1 Validation Case

The validity of FLM-SD.NS (single grid version) in regard to subsonic laminar flow has already been shown successfully for a harmonically pitching NACA0012 airfoil [20], with further investigations having been performed for the transonic flow regime in [11]. Due to the lack of turbulence modelling and the consequential restriction to low Reynolds number flow, no unsteady shock boundary layer interaction could be observed in the past simulations. With the implementation of the turbulent small disturbance Navier-Stokes code, such test cases have now become accessible.

For the initial validation of FLM-SD.NS (multi-grid version) at flight realistic Reynolds numbers the transonic experimental test case CT8 from AGARD-R-702 [8] is considered: A NACA 64A010 airfoil performs a harmonic incidence motion as governed by

$$\alpha(\tau_s) = \alpha_0 + \Delta\alpha \cdot \sin(k_{red} \cdot \tau_s), \qquad (83)$$

with the reference angle of attack α_0 and the amplitude $\Delta\alpha$ (pitch axis at 25% chord length c_r). Tab. 1. summarizes the case parameters.

Ma_∞	Re_∞	α_0	$\Delta\alpha$	k_{red}
0.8	$12.5 \cdot 10^6$	0.0°	0.5°	0.2

Table 1 NACA 64A010 CT8 parameters

The reduced frequency is defined through $k_{red} = k/\sqrt{\gamma}Ma_\infty = 2\pi c_r f/u_\infty$, with the corresponding characteristic time being $\tau_s = \sqrt{\gamma}Ma_\infty\tau$. In this context, the dimensional frequency $f\,[s^{-1}]$, chord length $c_r\,[m]$ and the freestream velocity $u_\infty\,[ms^{-1}]$ are supplied through the experimental setup.

Discretization of the computational domain takes place with an elliptically smoothed structured mesh in C-topology consisting of 384 cells in circumferential and 96 cells in surface normal direction. The symmetrical airfoil contour is digitized with 128 cells per side. An off-body distance of $1 \cdot 10^{-5} c_r$ for the first grid line ensures a $y^+ < 6$ as required by the Spalart-Allmaras turbulence model for viscous sublayer resolution. Additionally, cell density is increased in proximity to the airfoil contur, where shock appearance is anticipated. Both reference and deformed extremum grid are equivalent in their properties.

Applying FLM-SD.NS to the unsteady flow problem, a four level V-symmetric multi-grid cycle is selected for the solution process. Per multi-grid cycle dual iterations on the finest and coarsest grid levels in combination with a single iteration on each of the two intermediary levels allow for optimal convergence. The frequency domain calculation is terminated after both the L_2-normalized density and Spalart-Allmaras working variable residuals have dropped below $1 \cdot 10^{-5}$. For the comparative time-accurate simulation of the CT8 test case with FLM-NS three oscillations are computed in order to eliminate transient phenomena, each discretized with 100 physical time intervalls. Multi-grid settings and abort criteria are equivalent to the FLM-SD.NS solution procedure. Both numerical methods are employed on a Linux operating Intel® Pentium IV personal computer clocked at 2.66 GHz.

4.2 Evaluation and Discussion

In order to assess the capability of FLM-SD.NS to accurately predict unsteady air loads, pressure and skin friction distributions on the airfoil's contour are investigated at first. As the experimental data provided in AGARD-R-702 [8] is limited to zeroth and first harmonic pressure coefficients, c_p^0 and c_p^1 respectively, skin friction values (c_f^0, c_f^1) are supplemented through FLOWer calculations [13]. The algebraic turbulence model according to Baldwin-Lomax [3] is employed. Developed at DLR, FLOWer is a validated time accurate Reynolds-averaged Navier-Stokes solver in widespread German use. Results of FLM-SD.NS in comparison to FLM-NS, FLOWer solutions and experimental data are composited in Fig. 1. Furthermore, an inviscid small disturbance solution computed with FLM-SDEu [12] is supplied for the purpose of evaluating the impact of viscous effects.

Resulting from Fourier analysis of the time-accurate FLM-NS and FLOWer solutions, a comparison of c_p^0 and c_f^0 to the FLM-SD.NS counterparts reveals only slight deviations. This serves as an indication that the first and higher harmonics of the unsteady flow response have little influence on the zeroth harmonic. Therefore, the mean flow shows good conformity with the steady state solution, which acts as input for the linearized method. Consequently, if the negligibility of higher harmonics holds, CT8 becomes a valid test case for FLM-SD.NS, as flow decomposition into a mean and linear perturbation part is possible. Disparity between the inviscid steady state solution used as input for FLM-SDEu and the viscous solutions is evident for the shock region. Initiation of the shock is located farther downstream with a stronger gradient and less post shock dampening, due to the absence of boundary layer interaction.

Real and imaginary parts of the first harmonic pressure c_p^1 and skin friction distributions c_f^1 computed with FLM-SD.NS exhibit good agreement with their Fourier analyzed FLM-NS and FLOWer equivalents. However, larger differences between the viscous numerical methods occur at the shock location, with FLM-SD.NS predicting a much higher peak value than the two non-linear methods. Good correspondence to the c_p^1 measured values is also observed outside of the shock region. In vicinity of the shock it becomes difficult to assess local solution accuracy, as only one experimental data point lies within its extent. As to be expected, the c_p^1 distribution calculated with FLM-SDEu retains the shock characteristic peak farther downstream than the other data, as the disagreeing inviscid steady state solution has served as its input. The significantly stronger and narrower peak at the shock location is also prominent, again being attributed to the absence of a boundary layer.

In and out of phase components of the lift ($Re\,c_l^1$, $Im\,c_l^1$) and pitching moment ($Re\,c_m^1$, $Im\,c_m^1$) coefficients are computed from the preceding distributions for both FLM-SD.NS and FLM-NS. The reference axis for the pitching moment coincides with the rotational axis of the incidence motion located at $25\%c_r$, with a positive moment defined as being tail-heavy. Summarized in Tab. 2, deviation of the small disturbance c_l^1 values from the corresponding non-linear ones is marginal, establishing good agreement. However, unfavoarable discrepancies in the range of 15% to 19% are identified for c_m^1, as the influence of shock overprediction through FLM-SD.NS becomes noticeable.

method	FLM-SD.NS	FLM-NS
$Re\,c_l^1/\Delta\alpha$	6.630	6.619
$Im\,c_l^1/\Delta\alpha$	−3.072	−3.021
$Re\,c_m^1/\Delta\alpha$	−0.426	−0.358
$Im\,c_m^1/\Delta\alpha$	−0.149	−0.176

Table 2 NACA 64A010 CT8: Comparison of the computed global coefficients

Recompositing the global coefficients' first harmonic values for the time domain in conjunction with their respective mean counterparts, c_l^0 and c_m^0, yields the c_l and c_m progression over the incidence motion (Fig. 2). In order to il-

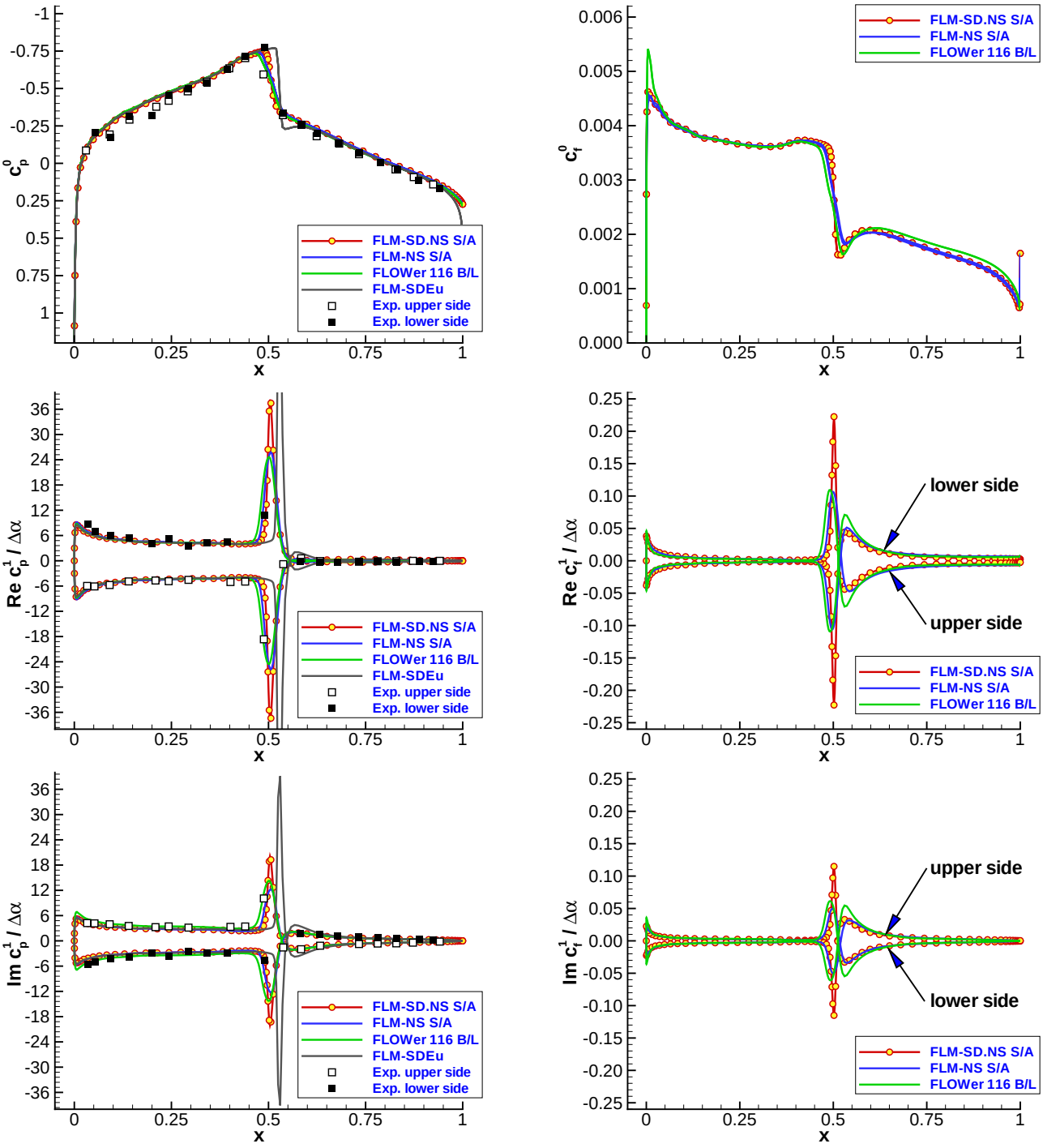

Fig. 1 Comparison of the pressure coefficient (c_p^0, c_p^1) and skin friction coefficient (c_f^0, c_f^1) distributions for NACA 64A010 CT8 ($Ma_\infty = 0.8$, $Re_\infty = 12.5 \cdot 10^6$, $\alpha_0 = 0.0°$, $\Delta\alpha = 0.5°$, $k_{red} = 0.2$)

lustrate the transient process characteristic for a non-linear FLM-NS solution, the coefficient development over all three cycles is plotted. Having achieved periodicity in the last oscillation, it is selected for comparative purposes. For both coefficient evolutions FLM-SD.NS exhibits satisfactory conformity with the time dependent hystereses computed through FLM-NS and FLOWer, the small disturbance c_l composite being almost identical to the respective FLM-NS calculated

progression. In contrast the small disturbance solution for c_m agrees better with the respective FLOWer hysteresis than with the one calculated by FLM-NS.

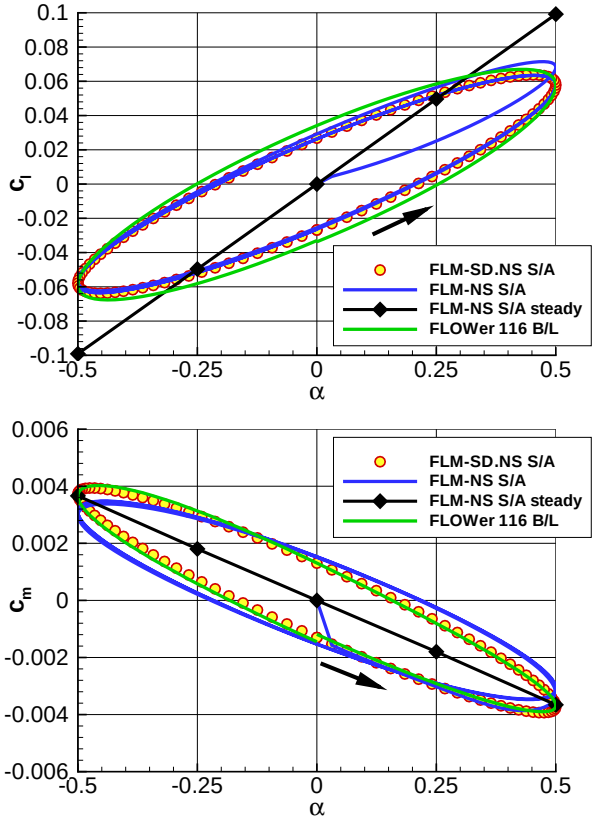

Fig. 2 NACA 64A010 CT8 lift and moment coefficient evolution over the incidence motion

Regarding the CT8 case, FLM-SD.NS surpasses FLM-NS by a factor off 11.7 in simulation speed (Tab. 3), with absolute CPU time being at 1.05 hours for the small disturbance method. The trade off for the enhanced efficiency lies in higher storage requirements, with FLM-SD.NS allocating more than triple the amount of working memory (RAM) as FLM-NS. Performing single-grid computations of the CT8 with FLM-SD.NS and FLM-NS yields a reduced CPU time ratio of 5.2 between the two methods. It becomes evident that the acceleration due to the multi-grid technique does not transfer one-to-one between the small disturbance and non-linear implementations, the scheme being more powerful in combination with the psuedo-steady state solution process of FLM-SD.NS.

method	FLM-SD.NS	FLM-NS
CPU time [h]	1.1 $(3.7)^{SG}$	12.3 $(19.3)^{SG}$
RAM [GByte]	0.78	0.22

$(\ )^{SG}$: single-grid computation

Table 3 NACA 64A010 CT8: Comparison of the computational effort

On basis of the CT8 case a variation of the reduced frequency k_{red} is performed for further investigation of FLM-SD.NS performance. Ten distinct frequencies between $k_{red} \approx 0$ and $k_{red} = 2.0$ have been calculated with both FLM-SD.NS and FLM-NS. First harmonics of the unsteady lift and moment coefficient are plotted over the reduced frequency in Fig. 3. Real and imaginary parts of c_l^1 exhibit good conformity between the linearized and non-linear method over the complete frequency spectrum. Larger deviations are apparent for c_m^1, with the real part being affected in the lower frequency range especially, as the discrepancy in shock prediction widens.

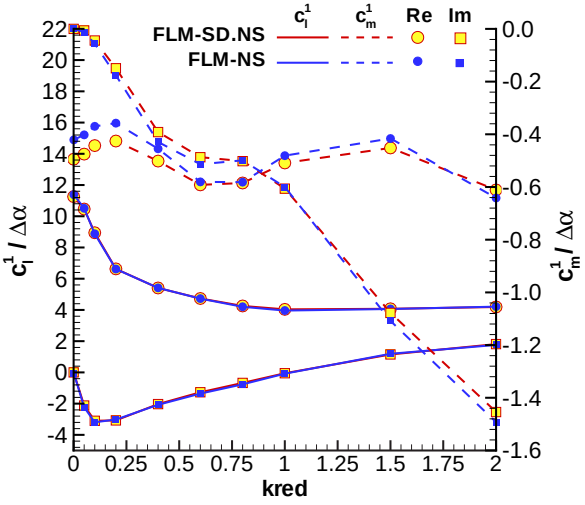

Fig. 3 Influence of the reduced frequency k_{red} on lift and moment coefficient prediction

As can be seen in Fig. 4, with decreasing k_{red} the CPU time ratio ζ between FLM-NS and

FLM-SD.NS increases significantly. This is primarily attributed to the non-linear solver's reduced performance at low frequencies, convergence behavior of FLM-SD.NS exhibiting far less variation over the frequency spectrum.

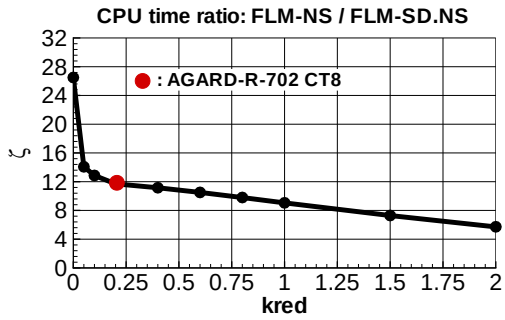

Fig. 4 Relative computational effort at distinct reduced frequencies k_{red}

5 Conclusions

With FLM-SD.NS an efficient method for calculating unsteady airloads on the basis of the small disturbance Navier-Stokes equations has been presented. Incorporation of a linearized formulation of the Spalart-Allmaras one-equation turbulence model allows the simulation of high Reynolds number flows, as was demonstrated for a harmonically pitching airfoil characterized by unsteady shock boundary layer interaction. Overall good to satisfactory agreement in the results between the small disturbance and the comparative time-accurate methods, as well as the experimental data, was observed. Reductions in computational time up to an order of magnitude document the efficiency and validity of the small disturbance approach. The developed implicit pseudo-time stepping scheme in conjunction with a multi-grid technique contributes significantly to the enhancement of performance. In the near term an extension of code validation to the two-dimensional turbulent sub- and supersonic flow regime will have to be realized. Ultimately, application of the small disturbance Navier-Stokes method to wings of various aspect ratio is envisioned.

References

[1] Acharya, M.: Measurements and predictions of a fully developed turbulent channel flow with imposed controlled oscillations. *Ph. D. Thesis*, Stanford University, 1975.

[2] Allen A., Weishäupl C., Laschka B.: Flap efficiency of a delta wing with an external store using an Euler code for small disturbances. 13. DGLR-STAB-Symposium, 12.-14. Nov. 2002 published in: *Notes on Numerical Fluid Mechanics and Multidisciplinary Design*, Vol. 87, NNFM, pp. 116-123.

[3] Baldwin, B. S., Lomax H.: Thin layer approximation and algebraic model for separated turbulent flows. *AIAA Paper 78-257*, NASA Ames Research Center, Moffett Field, CA.

[4] Blazek J.: Investigations of the implicit LU-SSOR scheme. *DLR-FB 93-51*, DLR Braunschweig, Jul. 1993.

[5] Chakravarthy S. R.: High resolution upwind formulations for the Navier-Stokes equation. *v. Karman Institute for Fluid Dynamics Lecture Series 1988-05*, Computational Fluid Dynamics, Mar. 7.-11., 1988.

[6] Clark W. S., Hall K. C.: A time-linearized Navier-Stokes analysis of stall flutter. *Journal of Turbomachinery*, Vol. 122, Jul. 2000, pp. 467-476.

[7] Cvrlje T., Breitsamter C., Weishäupl C., Laschka B.: Euler and Navier-Stokes simulation of two stage hypersonic vehicle longitudinal motions. *Journal of Spacecraft and Rockets*, Vol. 37. No. 2, Mar. - Apr. 2000.

[8] Davis S. D.: NACA64A010 (NASA Ames model) oscillatory pitching. *AGARD Report No. 702, Compendium of Unsteady Aerodynamic Measurements*, 1982.

[9] Hall K. C., Crawley E. F.: Calculation of unsteady flows in turbomachinery using the linearized Euler equations. *AIAA Journal*, Vol. 27, No. 6, 1989, pp. 777-787.

[10] Iatrou M., Weishäupl C., Laschka B.,: Entwicklung eines instationären Navier-Stokes-Verfahrens bei kleinen Störungen für aeroelastische Problemstellungen. *DFG-Zwischenbericht*, Technische Universität München, TUM-FLM-2002/9, 2002.

[11] Iatrou M., Weishäupl C., Laschka B.,: Entwicklung eines instationären Navier-Stokes-Verfahrens bei kleinen Störungen für aeroelastische Problemstellungen. *DFG-Abschlussbericht*, Technische Universität München, TUM-FLM-2003/27, 2003.

[12] Kreiselmaier E., Laschka B.: Small disturbance Euler equations: efficient and accurate tool for unsteady load predictions. *Journal of Aircraft*, Vol. 37, No. 5, Sept.-Oct. 2000, pp. 770-778.

[13] Kroll N.: *FLOWer installation and user handbook*, Institut für Entwurfsaerodynamik, DLR, 1998.

[14] Laschka, B.: Unsteady flows - fundamentals and applications. *AGARD Conference Proceedings No. 386, Unsteady Aerodynamics - Fundamentals and Applications to Aircraft Dynamics*, Göttingen, FRG, 1985.

[15] Lindquist D. R., Giles M. B.: Validity of linearized unsteady Euler equations with shock capturing. *AIAA Journal*, Vol. 32, No. 1, 1994, pp. 46-53.

[16] Morkovin, M. V.: Effects of compressibility on turbulent flows. *Mécanique de la Turbulence*, CNRS, 1962, pp. 367-380.

[17] Norris, H. L.: Turbulent channel flow with a moving wavy boundary. *Ph. D. Thesis*, Stanford University, 1975.

[18] Pechloff A.: Triple decomposition of the two-dimensional Navier-Stokes equations in Cartesian coordinates and linearization for small disturbances. *technical report*, Technische Universität München, TUM-FLM-2001/4, 2001.

[19] Pechloff A.: An implicit method for solving the small disturbance Navier-Stokes equations. *technical report*, Technische Universität München, TUM-FLM-2002/21, 2002.

[20] Pechloff A., Iatrou M., Weishäupl C., Laschka B.: The small disturbance Navier-Stokes equations: development of an efficient method for calculating unsteady air loads. 13. DGLR-STAB-Symposium, 12.-14. Nov. 2002 published in: *Notes on Numerical Fluid Mechanics and Multidisciplinary Design*, Vol. 87, NNFM, pp. 278-285.

[21] Petrie-Repar P.: Development of an efficient linearised Navier-Stokes flow solver for turbomachinery applications. 13. DGLR-STAB-Symposium, 12.-14. Nov. 2002 published in: *Notes on Numerical Fluid Mechanics and Multidisciplinary Design*, Vol. 87, NNFM, pp. 286-293.

[22] Sickmüller U., Pechloff A., Weishäupl C., Laschka B.: Aerodynamische Untersuchungen eines Deltaflügels bei verschiedenen Eigenformen mittels eines Euler-Verfahrens bei kleinen Störungen. *DGLR.2001-065*, Deutscher Luft- und Raumfahrtkongress 2001, Hamburg, 17.-20. Sept. 2001.

[23] Spalart P. R., Allmaras S. R.: A one-equation turbulence model for aerodynamic flows. *AIAA-92-0439*, 30th Aerospace Sciences Meeting & Exhibt, Jan. 6.-9., 1992 / Reno, NV.

[24] Telionis, P. D.: *Unsteady viscous flows.* Springer-Verlag, 1981.

[25] Weishäupl C., Laschka B.: Small disturbance Euler-simulations for unsteady flows of a delta wing due to harmonic oscillations. Accepted for publication in *Journal of Aircraft*, 2004.